J. Am. Soc. Mass Spectrom. (2019) 30:1491–1502
DOI: 10.1007/s13361-019-02214-6

RESEARCH ARTICLE

General Mechanism of C_α–C Peptide Backbone Bond Cleavage in Matrix-Assisted Laser Desorption/Ionization In-Source Decay Mediated by Hydrogen Abstraction

Daiki Asakawa

National Metrology Institute of Japan (NMIJ), National Institute of Advanced Industrial Science and Technology (AIST), Tsukuba, Ibaraki, Japan

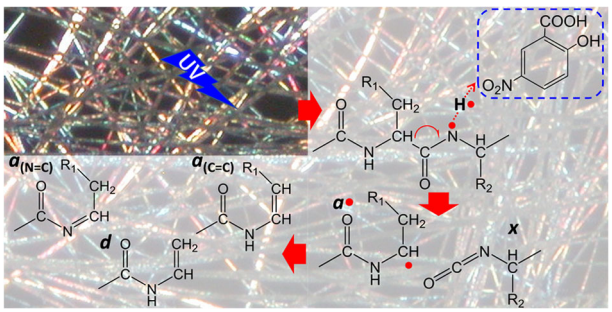

Abstract. Nitrogen-centered and β-carbon–centered hydrogen-deficient peptide radicals are considered to be intermediates in the matrix-assisted laser desorption/ionization in-source decay (MALDI-ISD)–induced C_α–C bond cleavage of peptide backbones when using an oxidizing matrix. To understand the general mechanism of C_α–C bond cleavage by MALDI-ISD, I study the fragmentation of model peptides and investigate the fragment formation pathways using calculations with density functional theory and transition state theory. The calculations indicate that the nitrogen-centered radical immediately undergoes C_α–C bond cleavage, leading to the formation of an *a*•/*x* fragment pair. In contrast, the dissociation of the β-carbon–centered radical is kinetically feasible under MALDI-ISD conditions, leading to the formation of an *a*/*x*• fragment pair. To discriminate these processes, I focus on the yield of *d* fragments, which originate from *a*• radicals through radical-induced side-chain loss, not from *a* fragments. The C_α–C bond cleavage on the C-terminal side of the carbamidomethylated cysteine residue is found to produce *d* fragments instead of *a* fragments. According to the calculation of the rate constant, the corresponding fragmentation occurs within 1 ns. The intense signal arising from *d* fragments and the lack of or weak signal from *a* fragments strongly suggest that the C_α–C bond cleavage occurs through a nitrogen-centered radical intermediate. In addition to the side-chain loss, the resulting *a*• radical undergoes hydrogen atom abstraction by the matrix. The results for a deuterium-labeled peptide indicate that the matrix abstracts a hydrogen atom from either the amide nitrogen or the β-carbon.

Keywords: MALDI-ISD, Nitrogen-centered peptide radical, C_α–C bond cleavage, Side-chain loss

Received: 5 March 2019/Revised: 2 April 2019/Accepted: 2 April 2019/Published Online: 30 May 2019

Introduction

Matrix-assisted laser desorption/ionization mass spectrometry (MALDI-MS) is a major analytical tool for the characterization of proteins [1]. An important advantage of MALDI is that intact peptide ions can be produced without abundant fragmentation, which facilitates rapid characterization of a protein digest. Furthermore, the use of specific reducing matrices such as 2,5-dihydroxybenzoic acid [2], 2-aminobenzoic acid [3], and 1,5-diaminonaphthalene (1,5-DAN) [4] can cause in-source decay (ISD) during MALDI experiments. In particular, the most impressive of these matrices is 1,5-DAN, which efficiently produces fragment ions and allows rapid characterization of the sequence of intact proteins [5]. MALDI-ISD is initiated by laser-induced hydrogen radical transfer from the matrix to the analyte peptide [6, 7], which has been suggested to occur via hydrogen bonding between the peptide and the matrix prior to desorption [8]. The resulting aminoketyl radical intermediate eventually undergoes N–C_α bond cleavage, leading to the formation of a *c*′/*z*• fragment pair

Electronic supplementary material The online version of this article (https://doi.org/10.1007/s13361-019-02214-6) contains supplementary material, which is available to authorized users.

Correspondence to: Daiki Asakawa; *e-mail:* d.asakawa@aist.go.jp

[9, 10]. Subsequently, the radical *z*• fragment either reacts with the matrix or undergoes further fragmentation to give various fragments such as, *z*′, *z*, *w*, and [*z* + matrix] [11, 12]. Because *z*′ fragments often appear as intense peaks, protein sequencing by MALDI-ISD is performed by interpreting mass differences between series of consecutive *c*′ and *z*′ ions. To obtain accurate mass differences, MALDI-ISD employing a Fourier transform ion cyclotron resonance (FTICR) mass spectrometer was recently developed [13–15]. Additionally, a MALDI-ISD–based pseudo-MS^3 method, that is mass selection of ISD ions followed by fragmentation with post-source decay, provides information on the identity of the C- and N-terminus of the protein and enables direct identification of a target protein in a mixture [16–19]. Moreover, MALDI-ISD preferentially produces *c*′ and *z*′ fragments without degradation of labile post-translational modifications, so the locations of phosphorylation [20], *O*-glycosylation [21], and polyethylene glycosylation [22] in proteins are determined. Consequently, MALDI-ISD is becoming increasingly important in the field of proteomics, and this is likely to continue.

In contrast to the N–C_α bond cleavage, the cleavage of the C_α–C bond was recently found to occur when 5-nitrosalicylic acid (5-NSA) was used as an oxidizing matrix for MALDI-ISD [23]. MALDI-ISD with 5-NSA permits identification of phosphorylated and isoaspartate residues in peptides [24, 25]. More recently, hydroxy-nitrobenzoic acid isomers [26–28], 7,7,8,8-tetracyanoquinodimethane derivatives [29], and 4-nitro-1-naphthol (4,1-NNL) [30] were reported to efficiently produce fragment ions due to a C_α–C bond cleavage. Regarding the mechanism, hydrogen abstraction from the peptide by the matrix produces a hydrogen-deficient peptide radical intermediate, which undergoes C_α–C bond cleavage. Because hydrogen abstraction can occur at all residues with similar probability, the C_α–C bond cleavage by MALDI-ISD is less prone to specific bond cleavages. However, as exceptions, the presence of proline (Pro), sarcosine (Sar), and glycine (Gly) residues was reported to affect the C_α–C bond cleavage efficiency [31]. We found that the C_α–C bond cleavage on the N-terminal side of the Pro and Sar residues did not occur; instead, fragments due to a peptide bond cleavage were observed [31]. The lack of fragments due to the C_α–C bond cleavage is likely to arise from the lack of amide hydrogen on the peptide backbone of the Pro and Sar residues. Consequently, the C_α–C bond cleavage by MALDI-ISD with an oxidizing matrix is assumed to be initiated by abstraction of an amide hydrogen from the peptide. Upon formation of the nitrogen-centered peptide radical, the cleavage of C_α–C bonds located on the N- and C-terminal sides of the radical site provides *a*•/*x* and *a*/*x*• fragment pairs, respectively, and the corresponding fragmentation pathways are illustrated in Scheme 1a, b, respectively. As described above, the presence of the Pro and Sar residues suppresses the cleavage of C_α–C bonds at the N-terminal side of Pro and Sar residues, because these residues do not contain an amide hydrogen on the peptide backbone. These results indicate that the resulting nitrogen-centered radical undergoes cleavage of C_α–C bonds located on the N-terminal side of the radical site (Scheme 1a)

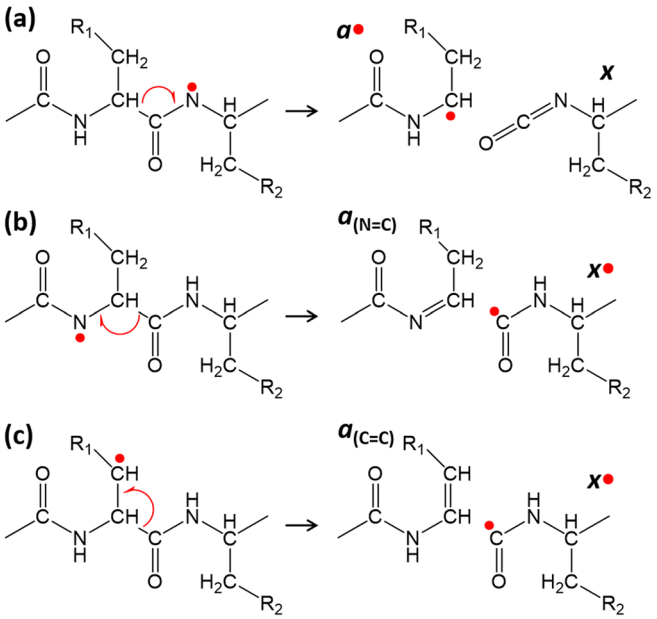

Scheme 1. Proposed mechanism of C_α–C bond cleavage by MALDI-ISD. (**a**) *a*•/*x* fragment pair formation from a nitrogen-centered radical by the cleavage of C_α–C bonds located on the N-terminal side of the radical site. (**b**) $a_{(N=C)}$/*x*• fragment pair formation from a nitrogen-centered radical by the cleavage of C_α–C bonds located on the C-terminal side of the radical site. (**c**) $a_{(C=C)}$/*x*• fragment pair formation from a β-carbon–centered radical

and the C_α–C bond at the N-terminal side of Pro and Sar residues are not cleaved because the Pro and Sar residues cannot form the nitrogen-centered radical [31]. In addition, the density functional theory (DFT) calculation also suggests that the C_α–C bonds located on the N-terminal side of the radical site in nitrogen-centered radicals are preferentially cleaved [32]. Therefore, I concluded that MALDI-ISD using an oxidizing matrix produces an *a*•/*x* fragment pair through a nitrogen-centered radical intermediate (Scheme 1a) [33, 34].

The pathway described in Scheme 1a is considered to be induced by the fragmentation techniques involving electron ejection from multiple deprotonated peptides, such as electron detachment dissociation (EDD) [35], negative electron transfer dissociation (NETD) [36]. These techniques result in the formation of a charge-reduced peptide anion that contains a radical site on the carboxyl group of the side chain or C-terminal carboxyl group. Because the carboxyl group often interacts with hydrogen at the peptide bond, the resultant radical at the carboxyl group abstracts a hydrogen from the backbone amide nitrogen, leading to an *a*•/*x* fragment pair through a nitrogen-centered radical intermediate [37]. Therefore, MALDI-ISD using an oxidizing matrix would share some mechanistic similarities with EDD and NETD.

In contrast, the presence of the Gly residue affects the C_α–C bond cleavage efficiency, as in the case of the Pro residue [34]. Recently, Nagoshi et al. [30] focused on the low cleavage efficiency of C_α–C bonds at the C-terminal side of Gly residue. These authors focused that the low fragmentation efficiency

arises from the lack of a β-carbon atom in the Gly residue, and they suggested the MALDI-ISD process involves a β-carbon–centered radical intermediate (Scheme 1c). The site of hydrogen abstraction from peptides was also investigated by these authors using a peptide with deuterium labeling at the side chain of the alanine residue, Ala-(d_3). MALDI-ISD of the deuterium labelled peptide employing an oxidizing matrix produced *a* fragments containing two deuterium atoms, indicating that the formation of *a* ions involved deuterium abstraction from the side chain of the Ala-(d_3) residue. Because they assumed that MALDI-ISD involves C_α–C bond cleavage leading to *a*/*x*• fragment pair formation (Scheme 2b, c), intense signal of *a*-d_2 fragments originated from β-carbon–centered radical intermediates. According to this hypothesis, the generation of a β-carbon–centered radical intermediate is more favorable than the generation of a nitrogen-centered radical intermediate during the MALDI-ISD process. However, the authors did not consider the contribution of *a*•/*x* fragment pair formation through a nitrogen-centered radical (Scheme 1a), which, is concluded as the most probable pathway by my review articles [33, 34], as described above. Subsequently, the resulted *a*• radical immediately undergoes hydrogen atom abstraction by reaction with the matrix, and potential sites for this hydrogen abstraction are the amide nitrogen and β-carbon atoms (Scheme 2a). Consequently, *a*-d_2 fragments can be produced from nitrogen-centered radical intermediates by *a*•/*x* fragment pair formation (Scheme 1a) and subsequent deuterium abstraction from β-carbon atoms in *a*•-d_3 radicals (Scheme 2a).

To estimate the contribution of each of the pathways described in Scheme 1 to the MALDI-ISD process, this article focuses first on DFT and transition state theory (TST) calculations that can be used to predict the mechanisms underlying the C_α–C bond cleavage, followed by a discussion of experimental and theoretical results. Subsequently, the formation mechanism of *d* fragments, which are often observed in MALDI-ISD mass spectra [26–29] is investigated. Such *d* fragments are believed to originate from *a*• radicals, as shown in Scheme 3 [26, 29], and their yield is found to be dependent on the transition state barrier to the side-chain loss of *a*• radicals. The joint experimental and computational study suggested that *a*•/*x* fragment pair formation through a nitrogen-centered radical intermediate (Scheme 1a) is the most probable pathway for MALDI-ISD employing an oxidizing matrix.

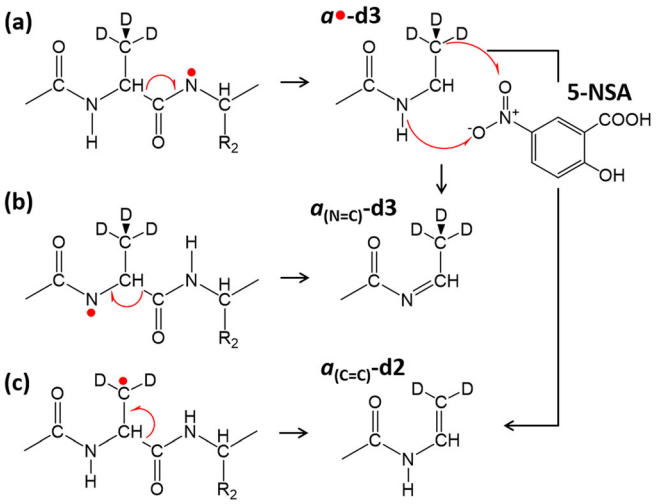

Scheme 2. Formation mechanism of $a_{(C=C)}$ and $a_{(N=C)}$ fragments originating from the cleavage of the C_α–C bond at the C-terminal side of Ala-(d_3) residue

Experimental

Materials

The peptide, substance P, was purchased from the Peptide Institute (Osaka, Japan), and all synthetic peptides were purchased from GenScript (NJ, USA). Table 1 shows detailed peptide information. 5-NSA and 4,1-NNL were purchased from Tokyo Chemical Industry (Tokyo, Japan). Ammonium bicarbonate, iodoacetamide, 3-hydroxy-2-nitrobenzoic acid (3H2NBA), and 3-hydroxy-4-nitrobenzoic acid (3H4NBA) were purchased from Wako Pure Chemical Industries (Osaka, Japan). All reagents were used without further purification. All solvents used were of HPLC grade quality, except for water, which was purified using a Milli-Q purification system (Millipore, Billerica, MA, USA). The conductivity of the purified water was 18.2 MΩ/cm.

MALDI-ISD Experiments

The peptides were dissolved in water to give a 50 μM solution. DCL-substance P was *S*-carbamidomethylated by 0.22 M iodoacetamide in a 100 μL solution of 0.1 M ammonium bicarbonate at pH 8.0 for 30 min at room temperature. The resultant mixture was removed by GL-Tip SDB (GL Sciences, Tokyo), and then, the eluted peptide solution was dried by centrifugal concentration. The matrices 5-NSA, 3H4NBA, 3H2NBA, and 4,1-NNL were used for the MALDI-ISD experiments. The matrix was dissolved in a 1:1 (*v*/*v*) water/acetonitrile mixture to give a 10 mg/mL solution. Then, 0.5 μL of the peptide aqueous solution (50 μM) and 0.5 μL of the matrix solution were deposited onto the MALDI plate. MALDI-ISD mass spectra were recorded using an AXIMA-CFR plus (Shimadzu/Kratos, UK). The analyzer was operated in linear mode with pulsed ion extraction. The laser power was optimized to obtain MALDI-ISD mass spectra that had high signal-to-noise ratios for the ISD ion peaks. In total, 500 shots were accumulated for each MALDI-ISD mass spectrum.

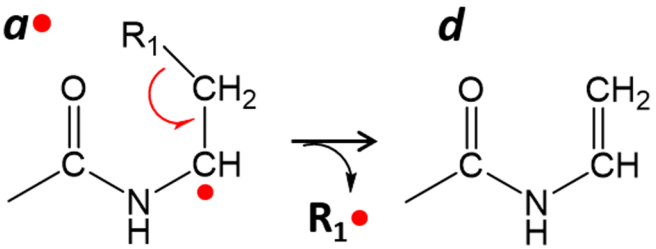

Scheme 3. Formation of *d* fragment from *a*• radical by radical-induced cleavage

Table 1. Monoisotopic mass (M_m), amino acid sequence, and composition of analyte peptides used

Peptide	M_m	Amino acid sequence	Composition
Substance P	1346.73	RPKPQQFFGLM-NH_2	$C_{63}H_{98}N_{18}O_{13}S$
NEI-substance P	1370.75	RPKPQFNEILM-NH_2	$C_{62}H_{102}N_{18}O_{15}S$
DCL-substance P	1345.70	RPKPQFDCLLM-NH_2	$C_{60}H_{99}N_{17}O_{14}S_2$

Calculations

All electron structure calculations were performed using the Gaussian 16 program [38]. The geometries of the radicals and molecules were obtained by optimization based on DFT calculations using the PW6B95D3 [39], which is recognized the best conventional global hybrid functional[40]. The structures were characterized by frequency calculations at local energy minima at the PW6B95D3/6-31+G(d,p) level. To establish the energetics for fragmentation, transition state geometries were also optimized at the PW6B95D3/6-31+G(d,p) level and confirmed by checking whether their vibrational frequencies had an imaginary part. The connections between the transition states and the reactants and intermediates were checked by intrinsic reaction coordinate analysis [40] starting from the transition state geometry. The harmonic frequencies obtained by frequency analysis were used to obtain zero-point energy corrections. The rate constants were calculated by the TST with one-dimensional semiclassical tunneling correction [41] assuming the asymmetric Eckart potential by using the Gaussian Post Processor program [42].

In the present study, Zubarev's notation was adopted for peptide fragment ions [43]. According to this notation, homolytic C_α–C bond cleavage yields the radical $a^\bullet$ and $x^\bullet$ fragments, and abstraction of a hydrogen atom from the $a^\bullet$ or $x^\bullet$ radical by matrix produces an a or x fragment, respectively.

Results and Discussion

Mechanism of C_α–C Bond Cleavage

To examine the processes occurring during MALDI-ISD that arise from hydrogen-deficient peptide radicals, the mechanisms underlying the C_α–C bond cleavage were investigated by DFT calculations. Because MALDI-ISD induces a similar fragmentation in both positive and negative ion modes, the MALDI-ISD process is considered as a charge remote fragmentation [34]. Consequently, first, I focused on the fragmentation process of a neutral peptide, and the effect of charge on the fragmentation process is then discussed.

To examine the fragmentation process, the hexapeptide-acetylated Ala-Ala-Ala-Ala-Ala-Ala-amide (AcA_6-NH_2) was used as a model system for the DFT calculations at the PW6B95D3/6-31+G(d,p) level. First, I searched for the model peptide conformation with the maximum number of intramolecular hydrogen bonds to find the global minimum-energy structure, because the peptide in the gas phase is stabilized by intramolecular hydrogen bonding. The polyalanine is known to adopt a conformation corresponding to the α-helix in the gas phase [44]. As expected, the DFT calculations yielded a minimum-energy conformation for AcA_6-NH_2 corresponding to the α-helix motif, which was then used as the initial conformation for the calculation of the fragmentation pathway. Then, I considered the cleavage of the C_α–C bond at Ala3-Ala4 to determine the most probable fragmentation pathway during MALDI-ISD; three competitive fragmentation pathways have been proposed, as shown in Scheme 1. According to the proposed processes, I calculated the fragmentation pathway for the C_α–C bond cleavage at Ala3-Ala4 in AcA_6-NH_2, as summarized in Figure 1.

Regarding the fragmentation pathway in Scheme 1a, hydrogen abstraction from the amide nitrogen at the Ala4 residue in AcA_6-NH_2 induced C_α–C bond cleavage at Ala3-Ala4. Consequently, [AcA_6-NH_2–H]• with a radical site on the amide nitrogen at Ala4 (R1a) was used as the initial conformation. As expected from the proposed mechanism in Scheme 1a, R1a produced an $a_3^\bullet/x_3$ fragment pair by the C_α–C bond cleavage

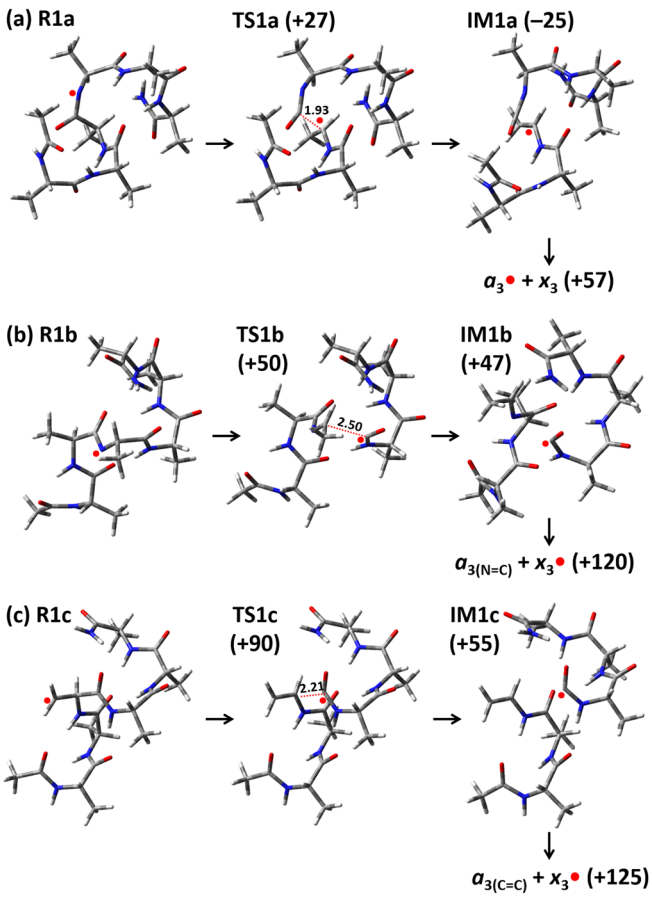

Figure 1. Cleavage mechanism of the C_α–C bond at Ala3-Ala4 in the hydrogen-deficient radical form of AcA_6-NH_2. Scheme 1 describes the reaction pathways. The relative energy levels (kJ mol^{-1}) were obtained from DFT calculations at the PW6B95D3/6-31+G(d,p) level and include zero-point vibrational energys

on the N-terminal side of the radical site. To obtain the transition state conformation during the C_α–C bond cleavage, the corresponding bond length was increased until an energy maximum was reached, and then, the obtained conformation was further optimized to find the saddle point. The calculated fragmentation pathway is shown in Figure 1a. The nitrogen-centered radical R1a undergoes C_α–C bond cleavage through the transition state TS1a, and the corresponding energy barrier was 27 kJ mol^{-1}. As a result, the a_3• and x_3 fragments produced were linked together via inter-fragment hydrogen bonding to provide the complex IM1a, which is more stable than R1a by 25 kJ mol^{-1}. The products a_3• and x_3 are 57 kJ mol^{-1} less stable than R1a.

In contrast, [AcA_6-NH_2–H]• with a radical site on the amide nitrogen at Ala3, R1b, undergoes cleavage at the C_α–C bond between the Ala3 and Ala4 residues by the fragmentation pathway shown in Scheme 1b. This fragmentation pathway was also examined by DFT calculations (Figure 1b). As expected from Scheme 1b, the cleavage of the C_α–C bond on the C-terminal side of the radical site produces an $a_{3(N=C)}/x_3$• fragment pair through the transition state TS1b, which is 50 kJ mol^{-1} higher in energy than the reactant, R1b. The product $a_{3(N=C)}$ has a double bond between the amide nitrogen and the α-carbon, and the counterpart x_3• radical contains a hydrogen-rich isocyanate radical in which the radical is delocalized over the isocyanate (N=C=O) group. The resultant $a_{3(N=C)}$ and x_3• are linked together via inter-fragment hydrogen bonding, producing the complex IM1b, and the energy of the $a_{3(N=C)}$ and x_3• formation was higher than that of R1b by 120 kJ mol^{-1}.

Upon forming the nitrogen-centered radical, the cleavage of the C_α–C bonds located on the N-terminal and C-terminal sides of the radical site occurs competitively, as shown in Scheme 1a, b. To determine the most probable fragmentation pathway during MALDI-ISD, I have, therefore, calculated the rate constants for the dissociation of R1a and R1b (Figure 2). As Figure 2 shows, the rate constant, k, is dependent on the temperature of the peptide radical. Because the temperature of the peptide ion is estimated to be around 900 K and 450 K in the early and late stages of MALDI plume, respectively [45], MALDI-ISD occurs at below 900 K. Regarding the timescale of the fragmentation, MALDI-ISD occurs in the ion source before applying the acceleration voltage, which is set to several hundred nanoseconds after laser irradiation. In consequence, MALDI-ISD occurs at a 100-ns timescale, indicating that a dissociation pathway with a rate constant of greater than 10^7 s^{-1} occurs during MALDI-ISD. According to Figure 2, the formation of an a_3•/x_3 fragment pair from R1a is faster than the formation of an $a_{3(N=C)}/x_3$• fragment pair from R1a at below 900 K, as shown in Figure 2. Therefore, the calculation strongly suggests that the nitrogen-centered radical attacks the C_α–C bond located on the N-terminal side of the radical site to provide an a•/x fragment pair, as indicated by the fragmentation pathway shown in Scheme 1a and Figure 1a. To confirm the dissociation rate of R1a and R2a, the DFT calculation is also performed with the M06-2X/6-31+G(d,p) level and the calculated rate constants are shown in the Supplemental Information, Figure S1. As in the case of Figure 2, Figure S1 indicates that the nitrogen-centered radical preferentially produced an a•/x fragment pair through the pathway shown in Scheme 1a. This result agrees with the conclusion drawn from the experimental results summarized in my previous review articles [33, 34], and the fragmentation process producing an $a_{3(N=C)}/x_3$• fragment pair through a nitrogen-centered radical intermediate (Scheme 1b) can be ruled out during the MALDI-ISD process.

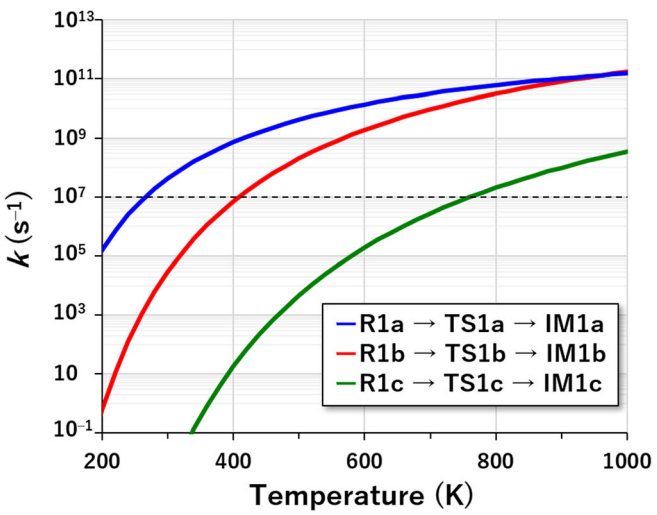

Figure 2. Rate constants for C_α–C bond dissociations in the hydrogen-deficient peptide radicals R1a, R1b, and R1c. The horizontal dashed line at $k = 10^7$ corresponds to dissociations occurring on the MALDI-ISD timescale of 100 ns

In contrast, Nagoshi et al. [30] proposed a C_α–C bond cleavage process involving a β-carbon–centered radical intermediate (Scheme 1c), as described in the Introduction Section. Herein, the β-carbon–centered radical at the radical site of the Ala3 residue, R1c, was used as the initial structure for the calculation of the $a_{3(C=C)}/x_3$• fragment pair formation. As Figure 1c shows, R1c produced the $a_{3(C=C)}/x_3$• fragment pair by C_α–C bond cleavage, and the corresponding transition state was TS1c, which is 90 kJ mol^{-1} higher in energy than the reactant, R1c. The resultant complex comprising $a_{3(C=C)}$ and x_3•, IM1c, is less stable by 55 kJ mol^{-1}, and the complete dissociation to $a_{3(C=C)}$ and x_3• fragments requires 125 kJ mol^{-1}. The rate constant for the corresponding fragmentation process is also plotted in Figures 2 and S1, which indicates that the dissociation of R1c through TS1c can occur on the timescale of the MALDI-ISD experiment (100 ns). Consequently, the $a_{3(C=C)}/x_3$• fragment pair can be generated if the β-carbon–centered radical is produced during MALDI-ISD.

The effect of charge on the MALDI-ISD process was then investigated. For this purpose, a hexapeptide containing a basic residue, acetylated Lys-Ala-Ala-Ala-Ala-Ala-amide ($AcKA_5$-NH_2), was used as a model system. The [$AcKA_5$-NH_2+H]$^+$ containing a protonated Lys residue, which is the most preferential site for protonation, was used as the initial structure in DFT calculations. As for AcA_6-NH_2 (Figure 1), the C_α–C bond cleavage at Ala3-Ala4 in [$AcKA_5$-NH_2+H]$^+$ was examined by DFT calculations, and the results are summarized in the Supplemental Information, Figure S2. By comparing Figures 1 and

S2, it can be seen that the transition state barriers obtained are similar, indicating that the presence of the extra proton does not influence the MALDI-ISD process. Consequently, MALDI-ISD can be viewed as a charge remote fragmentation, which further suggests that, in general, Figure 1 can be applied to both positive- and negative-ion MALDI-ISD processes. In summary, nitrogen-centered and β-carbon–centered radicals produced a_3•/x_3 and $a_{3(C=C)}$/x_3• fragment pairs, respectively, under MALDI-ISD experimental conditions, and the fragmentation producing an $a_{3(N=C)}$/x_3• fragment pair (Scheme 1b) is unfavorable during the MALDI-ISD process. Consequently, I then focused on the reaction of the a_3• radical with 5-NSA to investigate the production of $a_{3(N=C)}$ and $a_{3(C=C)}$ fragments.

Mechanism of $a_{(N=C)}$ and $a_{(C=C)}$ Fragment Formation

To determine the structure of the *a* fragment, Nagoshi et al. [30] investigated a peptide, RLGALGACLADLAEL, containing deuterium-labeled Ala residues, Ala(d_3), at positions 10 and 13. Both *a*-d_2 and *a*-d_3 fragments were produced from the deuterium-labeled peptide by MALDI-ISD using 4,1-NNL as the matrix [30]. Similarly, we have reported previously the MALDI-ISD mass spectrum of the deuterium-labeled peptide, RLGNQWA(d_3)VG(d_2)DLAE, when 5-NSA was used as the matrix [23]. In the previous article, we focused on the a_9 ion originating from a Cα–C bond cleavage at Gly(d_2)^9–Asp^{10}, and the results indicated that the formation of *a* ions did not involve hydrogen abstraction from the α-carbon [23]. Figure S3 in the Supplemental Information shows the MALDI-ISD mass spectrum of the deuterium-labeled peptide (the original data were previously published as Figure 5b in reference [23]). In the present work, I focused on Cα–C bond cleavage at Ala(d_3)^7–Val^8 residues, leading to the formation of the a_7 ion. As Figure S3 shows, MALDI-ISD of the deuterium-labeled peptide produced both a_7-d_2 and a_7-d_3, which are identified as $a_{(C=C)}$ and $a_{(N=C)}$ fragments, respectively. Although the abundance ratio of *a* ions containing Ala(d_2) and Ala(d_3) residues would be dependent on the matrix used and the sequence of the analyte peptide, the experimental results clearly indicate that MALDI-ISD employing an oxidizing matrix produces both $a_{(C=C)}$ and $a_{(N=C)}$ fragments (Scheme 2). Moreover, the MALDI-ISD mass spectrum clearly shows the *a* fragment without deuterium abstraction, *a*-d_3, which is not formed through a β-carbon–centered radical intermediate (Scheme 2). Consequently, the presence of an *a*-d_3 fragment can be viewed as evidence for the contribution of nitrogen-centered radicals in the MALDI-ISD process.

To assess the suitability of Scheme 2a, the formation of $a_{(N=C)}$ and $a_{(C=C)}$ by the reaction between *a*• radicals and 5-NSA was investigated using DFT calculations. For the purpose of these calculations, $a_{3(AcAAA)}$•, which is the product in Figure 1a, was used as a model. Figure 3 summarizes the calculated reaction pathways for the formation of $a_{(N=C)}$ and $a_{(C=C)}$ fragments. With regard to the formation of $a_{(N=C)}$, the interaction between the $a_{3(AcAAA)}$• and 5-NSA produced the complex R3a, and the corresponding binding

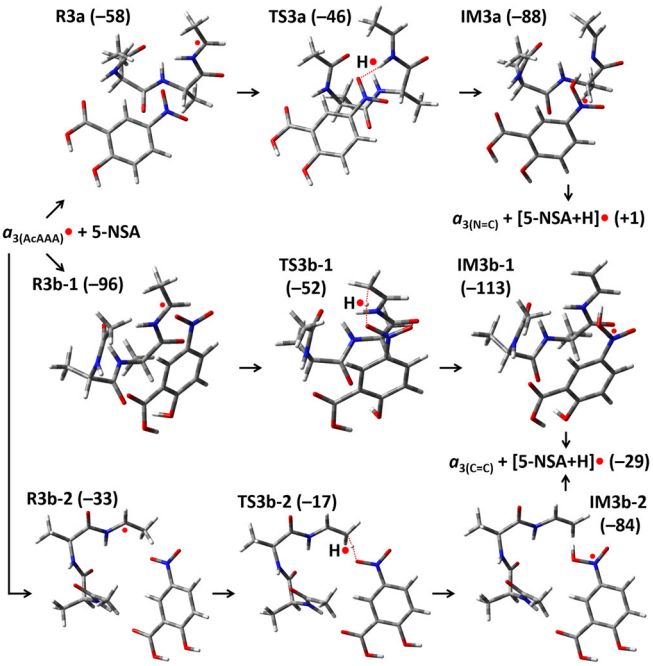

Figure 3. Mechanism of the formation of $a_{3(N=C)}$ and $a_{3(C=C)}$ by the reaction between $a_{(AcAAA)}$• radicals and 5-NSA. Scheme 2a describes the reaction pathways. The relative energy levels (kJ mol^{-1}) were obtained from DFT calculations at the PW6B95D3/6-31+G(d,p) level and include zero-point vibrational energys

energy was 58 kJ mol^{-1}. Hydrogen transfer from the amide nitrogen in $a_{3(AcAAA)}$• to the nitro group in 5-NSA produced an $a_{3(N=C)}$ fragment through the transition state TS3a, which is 12 kJ mol^{-1} higher in energy than R3a.

In contrast to R3a, the most stable complex consisting the $a_{3(AcAAA)}$• and 5-NSA is R3b, which is 96 kJ mol^{-1} more stable than the reactants. An $a_{3(C=C)}$ fragment is formed by the hydrogen abstraction from the β-carbon in $a_{3(AcAAA)}$• through the transition state TS3b-1, and the corresponding barrier is 44 kJ mol^{-1}. Although TS3b-1 is more stable than TS3a, reaction barrier for the formation of $a_{3(C=C)}$ is higher than $a_{3(N=C)}$. In contrast, R3b-2 is another conformation of the complex, in which $a_{3(AcAAA)}$• and 5-NSA are linked together via a hydrogen bond between the amide hydrogen in $a_{3(AcAAA)}$• and the carboxyl oxygen in 5-NSA. R3b-2 is 63 kJ mol^{-1} less stable than R3b-1. R3b-2 produced $a_{3(C=C)}$ through the transition state TS3b-2, and the corresponding barrier is 16 kJ mol^{-1}. Although the transition state barrier for the hydrogen transfer is dependent on the conformation of the complex consisting the $a_{3(AcAAA)}$• and 5-NSA, the transition state for the formation of both $a_{3(N=C)}$ and $a_{3(C=C)}$ is more stable than that of the reactants (free $a_{3(AcAAA)}$• and 5-NSA). In consequence, the formation of the $a_{(N=C)}$ and $a_{(C=C)}$ fragments can be considered to proceed as a barrierless reaction pathway, the reaction between $a_{3(AcAAA)}$• and 5-NSA would give both $a_{(N=C)}$ and $a_{(C=C)}$ fragments.

In summary, the results for a deuterium-labeled peptide indicate that MALDI-ISD produced two different types of *a*

fragments, i.e., $a_{(N=C)}$ and $a_{(C=C)}$. Since both types of *a* fragment can be produced from nitrogen-centered radicals by the C_α–C bond cleavage and subsequent hydrogen abstraction, the fragmentation pathways shown in Scheme 1a, c cannot be discriminated by MALDI-ISD experiments with peptides containing a deuterium-labeled Ala residue.

Mechanism of d Fragment Formation

To discriminate between the fragmentation pathways shown in Scheme 1a, c, next, I focused on the *d* fragment, which is formed by the side-chain loss of an *a*• radical, as shown in Scheme 3, because $a_{(C=C)}$ cannot produce *d* fragments. MALDI-ISD using an oxidizing matrix was reported previously to induce a side-chain loss at Asp, Leu, and Ile residues [26–29]. In this study, substance P–related peptides were used as models to investigate the yield of *d* fragments, which can reflect the amount of *a*• radical produced by MALDI-ISD. Figure 4 shows the MALDI-ISD mass spectra of substance P, NEI-substance P, and DCL-substance P. Since substance P–related peptides contain basic Arg and Lys residues at positions 1 and 3, respectively, MALDI-ISD preferentially produced protonated *a* and *d* fragments. As Figure 4 shows, the side-chain loss of the *a*• radical occurred at the Gln, Glu, Asn, Asp, Leu, Ile, and Cys. In particular, intense signals of the d_7 and d_8 fragments were observed in the MALDI-ISD mass spectra of DCL-substance P instead of the a_7 and a_8 fragments (Figure 4c). This result indicates that MALDI-ISD effectively induces the side-chain loss of Asp and Cys residues. In contrast, *d* fragments originating from the C_α–C bond cleavage and subsequent side-chain loss of Phe, i.e., d_7 and d_8 of substance P, d_6 of NEI-substance P, and DCL-substance P, were absent.

To understand the formation mechanism of the *d* fragments, I calculated the dissociation rate of an *a*• radical with the sequence Ac-Ala-Ala-Xxx, where Xxx is Asp, Asn, Glu, Gln, Leu, Ile, Phe, or Cys. Based on the fragmentation mechanism in Scheme 3, the energy of the transition state and products of the dissociation were calculated (Table 2). The transition state barriers for the d_3 fragment formation were around 95–130 kJ mol^{-1}, except for *a*• radicals with the sequences Ac-Ala-Ala-Cys and Ac-Ala-Ala-Phe. The side-chain loss of the Cys residue required only 70 kJ mol^{-1}, and the fragmentation proceeded without transition state. In contrast, the transition state barrier for the side-chain loss of the Phe residue was 163 kJ mol^{-1}, which is higher than that of the other residues. In consequence, *a*• radicals originating from a cleavage on the C-terminal side of the Cys residue preferentially give *d* fragments compared with other residues. Indeed, MALDI-ISD mass spectrum of DCL-substance P shows an intense signal of d_8 fragment, which is formed by the cleavage of Cys-Leu bonds, compared with a_8 fragments (Figure 4c). The use of a different matrix, 4,1-NNL, is reported to show an intense signal of *d* fragments originating from the C_α–C bond cleavage on the C-terminal side of the Cys residue, and the abundance of corresponding *a* fragments is low [30].

Regarding the side-chain loss from *a*• radicals, I found that *S*-carbamidomethylation on the Cys residue decreases the required energy for the fragmentation. The transition state barrier for the side-chain loss of *a*• radical with the sequence Ac-Ala-Ala-Cys*, where Cys* indicates a carbamidomethyl Cys residue, was only 34 kJ mol^{-1} (Table 2). To estimate the yield of *d* fragments, the rate constants for the side-chain loss of a_3• radicals with an Ac-Ala-Ala-Xxx sequence, where Xxx is Cys*, Phe, Asp, Asn, Glu, Gln, Leu, or Ile, were calculated (Figure 5). Notably, the dissociation of $a_3{}^{\bullet}{}_{(AcAAC)}$ proceeds without a transition state barrier and the corresponding rate constant could not be estimated. Regarding the $a_3{}^{\bullet}{}_{(AcAAC^*)}$, the dissociation constant is ~ 10^9 s^{-1} at 450 K and ~ 10^{11} s^{-1} at 900 K, indicating that the corresponding dissociation occurs within 1 ns, even in late stages of MALDI plume. Because *a*• radicals originating from a cleavage on the C-terminal side of the Cys* residue immediately undergo side-chain loss, the *S*-carbamidomethylation of DC*L-substance P would enhance d_8 fragment formation and suppress a_8 fragment formation. Indeed, MALDI-ISD of DC*L-substance P with 5-NSA shows an intense signal of d_8 fragment, which can be understood by the high dissociation rate constant (Figure 6a). Subsequently, I have analyzed DC*L-substance P with recently reported matrices: 3H2NBA [28] and 4,1-NNL [30] (Figure 6b, c), to determine the influence of the matrix used for the yield of *d* fragments. As Figure 6 shows, the side-chain loss of the Cys* residue was efficiently induced and the d_8 fragment was observed as an intense signal for all tested matrices. In contrast, the abundance of a_8 fragment was very low. Because the *d* fragments originated from the *a*• radicals, the yield of d_8 fragments in the MALDI-ISD of DC*L-substance P reflects the amount of $a^{\bullet}{}_8$ radicals produced. In contrast, $a_{(C=C)}$ fragments produced through a β-carbon–centered radical intermediate could be estimated from the yield of a_8 fragments in the MALDI-ISD of DC*L-substance P, because the $a_{(C=C)}$ fragment does not produce *d* fragments. Indeed, the d_8 fragment is 10–20 times more abundant than the a_8 fragment in the MALDI-ISD mass spectra of DC*L-substance P (Figure 6). The intense signal of d_8 fragments originating from the cleavage of the C_α–C bond on the C-terminal side of Cys* residue indicates that fragmentation leading to *a*•/*x* fragment pairs preferentially occurs (Scheme 1a), which suggests further that, in general, Scheme 1a holds for C_α–C bonds that do not involve a Cys* residue.

Next, I focused on the reaction rates for the side-chain loss of other residues. As described above, the timescale and temperature of MALDI-ISD are estimated to be 100 ns and 900 K, respectively. Consequently, the fragmentations with rate constants greater than 10^7 s^{-1} at 900 K occur during MALDI-ISD. As Figure 5 shows, the rate constant for the side-chain loss of a_3• is around 10^7 s^{-1} at 900 K, except for Phe and Cys*. Therefore, the side-chain loss from these residues is kinetically feasible under MALDI-ISD conditions. As expected, both *a* and *d* fragments were produced by the C_α–C bond cleavage on the C-terminal side of Gln, Glu, Asn, Asp, Leu, and Ile residues. In contrast, the side-chain loss of the Phe residue did not occur during MALDI-ISD for all tested matrices, because the fragmentation is predicted to be too slow at 900 K. Consequently, the absence of *d* fragments originating from C_α–C

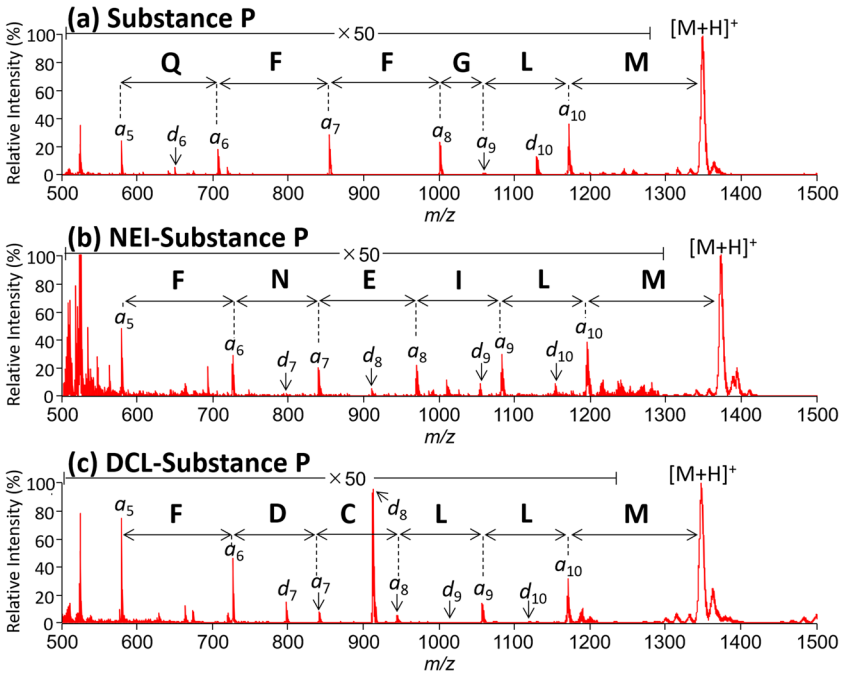

Figure 4. MALDI-ISD mass spectra of (**a**) substance P, (**b**) NEI-substance P, and (**c**) DCL-substance P. 5-NSA was used as the matrix

bond cleavage on the C-terminal side of the Phe residue can be understood by the low dissociation rate constant.

Then, I focused on the formation of *d* fragments originating from the cleavage on the C-terminal side of Asp residue, which are observed as intense signals in MALDI-ISD mass spectra of DCL-substance P and DC*L-substance P (d_7 fragment in Figures 4c and 6). As Figure 6 shows, the abundance of d_7 fragments originating from the side-chain loss of the Asp residue is dependent on the matrix used, which agrees with the previous report [26]. In contrast, MALDI-ISD of NEI-substance P produced medium or low ion yields of d_7 fragments, which originate from the C_α–C bond cleavage on the C-terminal side of Asn (Figure 4b). According to Figure 5, the dissociation rate constants of $a_3{}^{\bullet}{}_{(AcAAD)}$ and $a_3{}^{\bullet}{}_{(AcAAN)}$ are similar. Consequently, the intense signals arising from *d* fragments originating from the C_α–C bond cleavage on the C-terminal side of Asp cannot be explained by the unimolecular dissociation of *a*• radicals, and the side-chain loss of the Asp residue must occur through an alternative dissociation pathway. The proposed pathway is shown in Scheme 4, in which the hydrogen transfer from the carboxyl group on the Asp residue to 5-NSA potentially produced *d* fragments. To investigate the suitability of the proposed fragmentation pathway, DFT calculations were performed. As Figure 7 shows, the nitro group in 5-NSA binds with the carboxyl group on the Asp residue in $a_3{}^{\bullet}{}_{(AcAAD)}$, forming R7, and the corresponding binding energy is 41 kJ mol^{-1}. The hydrogen transfer from the

Table 2. Energy profiles for the side-chain loss of a_3• with an Ac-Ala-Ala-Xxx sequence, where Xxx is Cys, Glu, Gln, Asp, Asn, Leu, Ile, or Cys*

Reaction	TS	IM	Products
$a_3{}^{\bullet}{}_{(Ac\text{-}AAC)} \rightarrow d_3 + (SH)^{\bullet}$	–	–	70
$a_3{}^{\bullet}{}_{(Ac\text{-}AAQ)} \rightarrow d_3 + (CH_2CONH_2)^{\bullet}$	99	72	103
$a_3{}^{\bullet}{}_{(Ac\text{-}AAE)} \rightarrow d_3 + (CH_2COOH)^{\bullet}$	96	61	102
$a_3{}^{\bullet}{}_{(Ac\text{-}AAN)} \rightarrow d_3 + (CONH_2)^{\bullet}$	115	81	125
$a_3{}^{\bullet}{}_{(Ac\text{-}AAD)} \rightarrow d_3 + (COOH)^{\bullet}$	129	128	151
$a_3{}^{\bullet}{}_{(Ac\text{-}AAL)} \rightarrow d_3 + (C_3H_8)^{\bullet}$	117	78	106
$a_3{}^{\bullet}{}_{(Ac\text{-}AAI)} \rightarrow d_3 + (C_2H_5)^{\bullet}$	118	81	106
$a_3{}^{\bullet}{}_{(Ac\text{-}AAF)} \rightarrow d_3 + (C_6H_5)^{\bullet}$	163	153	191
$a_3{}^{\bullet}{}_{(Ac\text{-}AAC^*)} \rightarrow d_3 + (SCH_2CONH_2)^{\bullet}$	34	28	53

Scheme 3 describes the reaction pathways. The relative energy levels (kJ/mol) were obtained by DFT calculations at the PW6B95D3/6-31+G(d,p) level and include zero-point vibrational energy levels

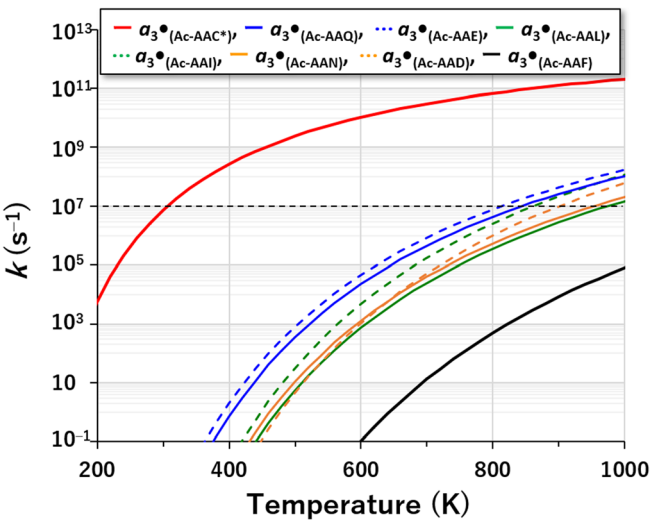

Figure 5. Rate constants for side-chain dissociations of a_3• with an Ac-Ala-Ala-Xxx sequence, where Xxx is Cys*, Phe, Asp, Asn, Glu, Gln, Leu, or Ile. The horizontal dashed line at $k = 10^8$ corresponds to dissociations occurring on the MALDI-ISD timescale of 10 ns

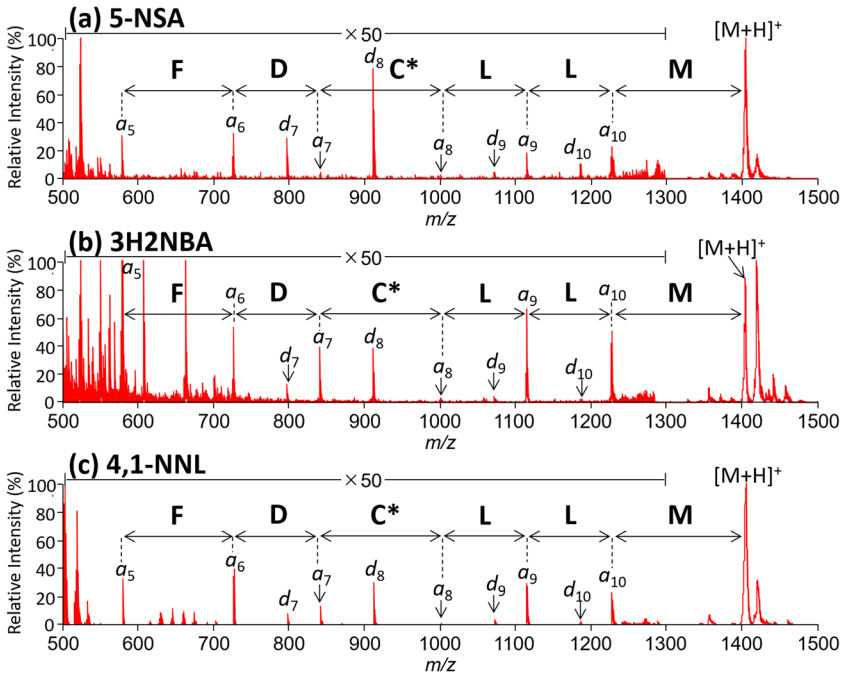

Figure 6. MALDI-ISD mass spectra of DC*L-substance P using different matrices. (**a**) 5-NSA. (**b**) 3H2NBA. (**c**) 4,1-NNL

carboxyl group on the Asp residue to 5-NSA proceeds through the transition state TS7, which is 6 kJ mol^{-1} more stable than the reactants (a_3•$_{(AcAAD)}$ and 5-NSA). As expected from Scheme 4, the hydrogen abstraction from a_3•$_{(AcAAD)}$ induces side-chain loss, leading to d_3 and CO_2. The products d_3, CO_2, and [5-NSA+H]• are 1 kJ mol^{-1} less stable than the reactants. The hydrogen abstraction–induced side-chain loss (Scheme 4) proceeded through a lower energetic pathway compared with the unimolecular side-chain loss (Scheme 3). Therefore, the intense signal arising from *d* fragments originating from the C_α–C bond cleavage on the C-terminal side of Asp can be explained by the reaction illustrated in Scheme 4.

Similarly, hydrogen abstraction from the side chain of the Asn residue in a_3•$_{(AcAAN)}$ radicals by 5-NSA would produce d_3 fragments and isocyanic acid (HNCO). However, the corresponding transition state was not obtained and the reaction is calculated to be exothermic by 50 kJ mol^{-1}. The hydrogen abstraction–mediated side-chain loss does not occur at the Asn residue due to the low stability of isocyanic acid. Both the experimental and theoretical results suggest that abstraction-induced side-chain loss only occurs for the Asp residue in *a*• radical.

Regarding the yield of *a* and *d* fragments, the d_7 fragment was more abundant than the a_7 fragment in the MALDI-ISD mass spectra of DCL-substance P and DC*L-substance P when 5-NSA was used as a matrix (Figures 4c and 6a). Similar results were obtained when 7,7,8,8-tetracyanoquinodimethane derivatives were used as the matrix [29]. Since *d* fragments originate from *a*• radicals, these experimental results strongly suggest that MALDI-ISD preferentially produces *a*•/*x* fragment pairs through the fragmentation pathway shown in Scheme 1a.

C-Terminal Side Fragments

In this section, C-terminal side fragments produced by MALDI-ISD are discussed. Figure S4 in the Supplemental Information shows the MALDI-ISD mass spectrum of the peptide PVKVYPNGAEDESAEAFR, and the original data were published previously as Figure 2d in reference 23. Since the peptide contains a basic Arg residue at the C-terminus, the C-terminal side fragments were selectively observed in the MALDI-ISD mass spectrum. As expected from the fragmentation pathway shown in Scheme 1a, *x* fragments were

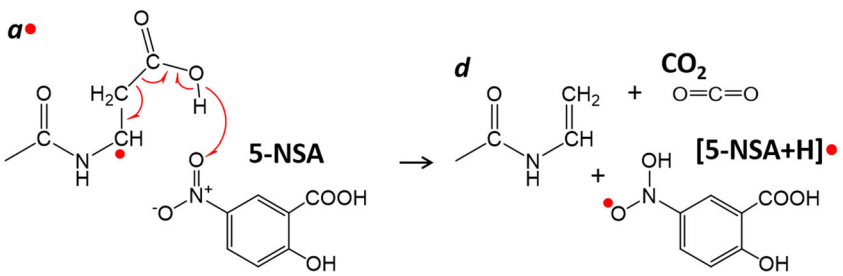

Scheme 4. Proposed mechanism of the side-chain loss of the Asp residue by hydrogen abstraction from the carboxyl group in the Asp residue to the nitro group in 5-NSA

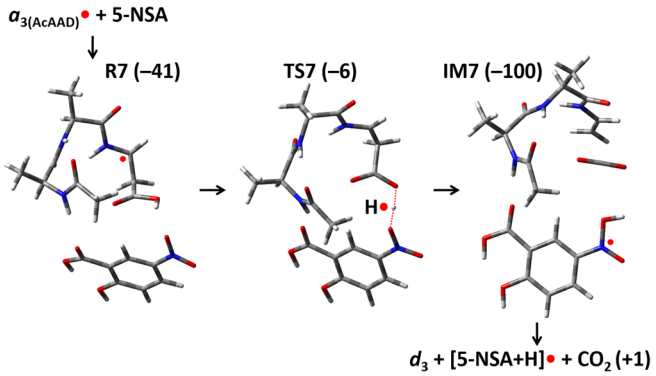

Figure 7. Calculated mechanism of the side-chain loss of the Asp residue by the reaction between the $a_{(AcAAD)}$• radical and 5-NSA. Scheme 4 describes the reaction pathways. The relative energy levels (kJ mol^{-1}) were obtained from DFT calculations at the PW6B95D3/6-31+G(d,p) level and include zero-point vibrational energys

observed as the C-terminal side fragments. In contrast, *x*• radicals, which are formed through Scheme 1c, would undergo further radical reactions due to their low stability.

Regarding the fragmentation of β-carbon–centered radical, the ultraviolet photodissociation (UVPD) of peptide with highly labile radical precursors is reported to produce the β-carbon–centered radical, which eventually undergoes C_α–C bond cleavage, leading to *a* fragments [46, 47]. In contrast, the counterpart *x*• radicals are unstable species which are never observed in the UVPD spectrum and *z*• radicals are observed instead of the *x*• radicals [47]. The results suggest that the *x*• radicals are stabilized by a loss of isocyanic acid, yielding *z*• radicals (Scheme 5). To assess the suitability of Scheme 5 for the MALDI-ISD process, the rate constants of the corresponding dissociation processes were calculated using an x_3• radical with a sequence of Xxx-Ala-Ala-NH_2, where Xxx is Gly, Ala, or Asn, as a model (Figure 8). The detailed fragmentation processes calculated by DFT are shown in the Supplemental Information, Figure S5. According to Figure 8, the rate constant for isocyanic acid loss from the *x*• radical is ~ 10^9 s^{-1} at 900 K, indicating that it is a kinetically feasible process under MALDI-ISD conditions. The *z*• radical is considered to be an intermediate of MALDI-ISD with a reducing matrix, and it produced *z*, *z*′, and *w* fragments by radical reactions in MALDI plume [34]. Consequently, the *x*• radical would be converted to *z*, *z*′, and *w* fragments through a *z*• radical

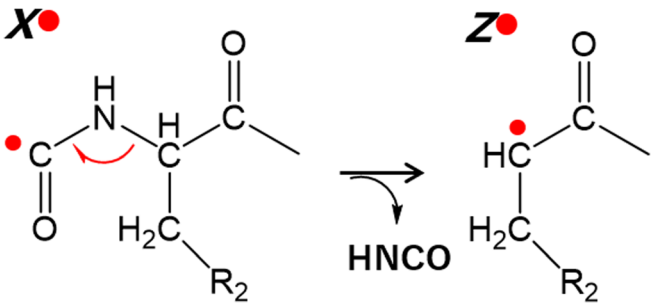

Scheme 5. Formation of *z*• radical from *x*• radical by radical-induced cleavage

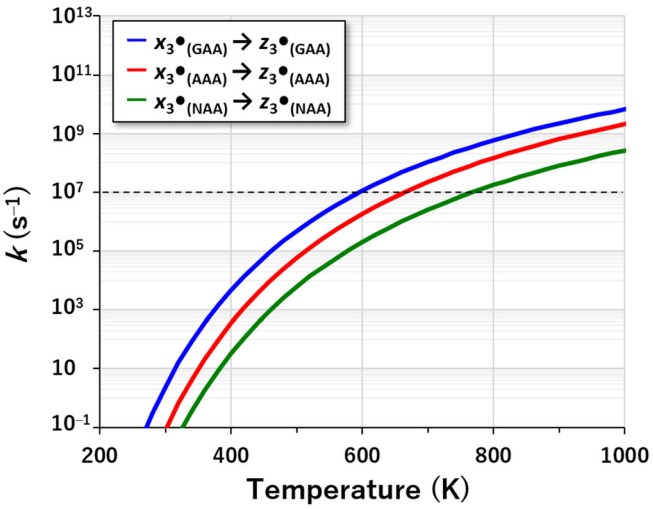

Figure 8. Rate constants for isocyanic acid loss from x_3• with an Xxx-Ala-Ala-NH_2 sequence, where Xxx is Gly, Ala, or Asn. The horizontal dashed line at $k = 10^7$ corresponds to dissociations occurring on the MALDI-ISD timescale of 100 ns

intermediate. With regard to the MALDI-ISD of the peptide PVKVYPNGAEDESAEAFR (Figure S4), the $z•_{10}$ and $z•_{11}$ radicals do not produce *w* fragments due to the lack of side chain in Gly and Ala residues. Consequently, $x•_{10}$ and $x•_{11}$ radicals produced the either *z* or *z*′ fragments. However, these fragments were absent from the spectrum shown in Figure S4, implying the absence of *x*• radicals during MALDI-ISD. These results also support the proposed mechanism of C_α–C bond cleavage through nitrogen-centered radicals (Scheme 1a).

In addition to *x* fragments, *w* and *y* fragments were observed in the spectrum shown in Figure S4. Since MALDI-ISD experiments with a reducing matrix also produced *w* and *y* fragments [11], the origin of these fragments might not be hydrogen-deficient radicals; however, the formation mechanism of these fragments was not ascertained. It should be noted that the spectrum in Figure S4 shows an x_{10} fragment, which is formed by a cleavage of on the C-terminal side of Gly residue, with moderate intensity, even though the abundance of *a* fragments originating from the C_α–C bond cleavage on the C-terminal side of the Gly residue is known to be low. Nagoshi et al. [30] concluded that the low abundance of the corresponding *a* fragment is due to the low efficiency of C_α–C bond cleavage, arising from the lack of β-carbon atoms. However, the counterpart *x* fragment is present in the MALDI-ISD mass spectrum, suggesting that the C-terminal side of the Gly residue might be cleaved during MALDI-ISD, as is the case for other C_α–C bonds. One explanation for the low abundance of *a*• radical originating from the cleavage of the C-terminal side of the Gly residue is that a further radical dissociation pathway is due to the low stability. This point will need future investigation.

Conclusion

Although nitrogen-centered and β-carbon–centered hydrogen-deficient peptide radicals are generally considered to be

intermediates in this process when using an oxidizing matrix, the results of the present joint experimental and computational study strongly suggest that peptide C_α–C bond cleavage occurs through nitrogen-centered radical formation. These results indicate that the oxidizing matrix preferentially abstracts a hydrogen atom from the amide nitrogen in peptide bond with subsequent radical-induced C_α–C bond cleavage, leading to the generation of an *a*•/*x* fragment pair. Then, the *a*• radical fragment either reacts with a matrix molecule or loses its side chain, leading to the *a* or *d* fragments. The yield of *d* fragments is dependent on the dissociation rate constant of the corresponding *a*• radical. In contrast, the matrix abstracts a hydrogen atom from either the amide nitrogen atom or the β-carbon atom in *a*• radical, producing an *a* fragment.

Acknowledgements

This work was supported by JSPS KAKENHI grant number 17K14508. The computations of molecular structures were performed by the Research Center for Computational Science, Okazaki, Japan.

Compliance with Ethical Standards

Conflict of Interest The author declares that he has no conflicts of interest.

References

1. Karas, M., Hillenkamp, F.: Laser desorption ionization of protein with molecular masses exceeding 10,000 daltons. Anal. Chem. **60**, 2299–2301 (1988)
2. Brown, R.S., Lennon, J.J.: Sequence-specific fragmentation of matrix-assisted laser-desorbed protein/peptide ions. Anal. Chem. **67**, 3990–3999 (1995)
3. Smargiasso, N., Quinton, L., De Pauw, E.: 2-Aminobenzamide and 2-aminobenzoic acid as new MALDI matrices inducing radical mediated in-source decay of peptides and proteins. J. Am. Soc. Mass Spectrom. **23**, 469–474 (2012)
4. Quinton, L., Demeure, K., Dobson, R., Gilles, N., Gabelica, V., De Pauw, E.: New method for characterizing highly disulfide-bridged peptides in complex mixtures: application to toxin identification from crude venoms. J. Proteome Res. **6**, 3216–3223 (2007)
5. Asakawa, D., Smargiasso, N., De Pauw, E.: Estimation of peptide N-C_α bond cleavage efficiency during MALDI-ISD using a cyclic peptide. J. Mass Spectrom. **51**, 323–327 (2016)
6. Takayama, M.: N-C_α bond cleavage of the peptide backbone via hydrogen abstraction. J. Am. Soc. Mass Spectrom. **12**, 1044–1049 (2001)
7. Kocher, T., Engstrom, Å., Zubarev, R.A.: Fragmentation of peptides in MALDI in-source decay mediated by hydrogen radicals. Anal. Chem. **77**, 172–177 (2005)
8. Asakawa, D., Calligaris, D., Smargiasso, N., De Pauw, E.: Ultraviolet laser induced hydrogen transfer reaction: study of the first step of MALDI in-source decay mass spectrometry. J. Phys. Chem. B. **117**, 2321–2327 (2013)
9. Asakawa, D., Smargiasso, N., Quinton, L., De Pauw, E.: Influences of proline and cysteine residues on fragment yield in matrix-assisted laser desorption/ionization in-source decay mass spectrometry. J. Am. Soc. Mass Spectrom. **25**, 1040–1048 (2014)
10. Asakawa, D., Takahashi, H., Iwamoto, S., Tanaka, K.: Fundamental study of hydrogen-attachment-induced peptide fragmentation occurring in the gas phase and during the matrix-assisted laser desorption/ionization process. Phys. Chem. Chem. Phys. **20**, 13057–13067 (2018)
11. Asakawa, D., Smargiasso, N., De Pauw, E.: Discrimination of isobaric Leu/Ile residues by MALDI in-source decay mass spectrometry. J. Am. Soc. Mass Spectrom. **24**, 297–300 (2013)
12. Asakawa, D., Smargiasso, N., Quinton, L., De Pauw, E.: Peptide backbone fragmentation initiated by side-chain loss at cysteine residue in matrix-assisted laser desorption/ionization in-source decay mass spectrometry. J. Mass Spectrom. **48**, 352–360 (2013)
13. Asakawa, D., Calligaris, D., Zimmerman, T.A., De Pauw, E.: In-source decay during matrix-assisted laser desorption/ionization combined with the collisional process in an FTICR mass spectrometer. Anal. Chem. **85**, 7809–7817 (2013)
14. Calligaris, D., Longuespée, R., Debois, D., Asakawa, D., Turtoi, A., Castronovo, V., Noël, A., Bertrand, V., De Pauw-Gillet, M.C., De Pauw, E.: Selected protein monitoring in histological sections by targeted MALDI-FTICR in-source decay imaging. Anal. Chem. **85**, 2117–2126 (2013)
15. Nicolardi, S., Switzar, L., Deelder, A.M., Palmblad, M., van der Burgt, Y.E.: Top-down MALDI-in-source decay-FTICR mass spectrometry of isotopically resolved proteins. Anal. Chem. **87**, 3429–3437 (2015)
16. Suckau, D., Resemann, A.: T^3-sequencing: targeted characterization of the N- and C-termini of undigested proteins by mass spectrometry. Anal. Chem. **75**, 5817–5824 (2003)
17. Calligaris, D., Villard, C., Terras, L., Braguer, D., Verdier-Pinard, P., Lafitt, D.: MALDI in-source decay of high mass protein isoforms: application to α- and β-tubulin variants. Anal. Chem. **82**, 6176–6184 (2010)
18. Debois, D., Bertrand, V., Quinton, L., De Pauw-Gillet, M.-C., De Pauw, E.: MALDI-in source decay applied to mass spectrometry imaging: a new tool for protein identification. Anal. Chem. **82**, 4036–4045 (2010)
19. Asakawa, D., Smargiasso, N., De Pauw, E.: New approach for pseudo-MS^3 analysis of peptides and proteins via MALDI in-source decay using radical recombination with 1,5-diaminonaphthalene. Anal. Chem. **86**, 2451–2457 (2014)
20. Lennon, J.J., Walsh, K.A.: Locating and identifying posttranslational modifications by in-source decay during MALDI-TOF mass spectrometry. Protein Sci. **8**, 2487–2493 (1999)
21. Hanisch, F.G.: Top-down sequencing of O-glycoproteins by in-source decay matrix-assisted laser desorption ionization mass spectrometry for glycosylation site analysis. Anal. Chem. **83**, 4829–4837 (2011)
22. Yoo, C., Suckau, D., Sauerland, V., Ronk, M., Ma, M.: Toward top-down determination of PEGylation site using MALDI in-source decay MS analysis. J. Am. Soc. Mass Spectrom. **20**, 326–333 (2009)
23. Asakawa, D., Takayama, M.: C_α-C bond cleavage of the peptide backbone in MALDI in-source decay using salicylic acid derivative matrices. J. Am. Soc. Mass Spectrom. **22**, 1224–1233 (2011)
24. Asakawa, D., Takayama, M.: Mass spectrometric characterization of phosphorylated peptides using MALDI in-source decay via redox reactions. J. Mass Spectrom. **47**, 180–187 (2012)
25. Yu, X., Sargaeva, N.P., Thompson, C.J., Costello, C.E., Lin, C.: In-source decay characterization of isoaspartate and β-peptides. Int. J. Mass Spectrom. **390**, 101–109 (2015)
26. Asakawa, D., Sakakura, M., Takayama, M.: Influence of initial velocity of analytes on in-source decay products in MALDI mass spectrometry using salicylic acid derivative matrices. Int. J. Mass Spectrom. **337**, 29–33 (2013)
27. Fukuyama, Y., Izumi, S., Tanaka, K.: 3-Hydroxy-4-nitrobenzoic acid as a MALDI matrix for in-source decay. Anal. Chem. **88**, 8058–8063 (2016)
28. Fukuyama, Y., Izumi, S., Tanaka, K.: 3-Hydroxy-2-nitrobenzoic acid as a MALDI matrix for in-source decay and evaluation of the isomers. J. Am. Soc. Mass Spectrom. **29**, 2227–2236 (2018)
29. Asakawa, D., Takayama, M.: Fragmentation processes of hydrogen-deficient peptide radicals in matrix-assisted laser desorption/ionization in-source decay mass spectrometry. J. Phys. Chem. B. **116**, 4016–4023 (2012)
30. Nagoshi, K., Yamakoshi, M., Sakamoto, K., Takayama, M.: Specific C_α-C bond cleavage of β-carbon-centered radical peptides produced by matrix-assisted laser desorption/ionization mass spectrometry. J. Am. Soc. Mass Spectrom. **29**, 1473–1483 (2018)
31. Asakawa, D., Takayama, M.: Specific cleavage at peptide backbone C_α-C and CO-N bonds during matrix-assisted laser desorption/ionization in-source decay mass spectrometry with 5-nitrosalicylic acid as the matrix. Rapid Commun. Mass Spectrom. **25**, 2379–2383 (2011)
32. Anusiewicz, I., Jasionowski, M., Skurski, P., Simons, J.: Backbone and side-chain cleavages in electron detachment dissociation (EDD). J. Phys. Chem. A. **109**, 11332–11337 (2005)

33. Asakawa, D.: 5-Nitrosalicylic acid as a novel matrix for in-source decay in matrix-assisted laser desorption/ionization mass spectrometry. Mass Spectrom. **2**, A0019 (2013)
34. Asakawa, D.: Principles of hydrogen radical mediated peptide/protein fragmentation during matrix-assisted laser desorption/ionization mass spectrometry. Mass Spectrom. Rev. **35**, 535–556 (2016)
35. Budnik, B.A., Haselmann, K.F., Zubarev, R.A.: Electron detachment dissociation of peptide di-anions: an electron–hole recombination phenomenon. Chem. Phys. Lett. **342**, 299–302 (2001)
36. Coon, J.J., Shabanowitz, J., Hunt, D.F., Syka, J.E.: Electron transfer dissociation of peptide anions. J. Am. Soc. Mass Spectrom. **16**, 880–882 (2005)
37. Kjeldsen, F., Silivra, O.A., Ivonin, I.A., Haselmann, K.F., Gorshkov, M., Zubarev, R.A.: C_{α}-C backbone fragmentation dominates in electron detachment dissociation of gas-phase polypeptide polyanions. Chem. Eur. J. **11**, 1803–1812 (2005)
38. Frisch, M. J., Trucks, G. W., Schlegel, H. B., Scuseria, G. E., Robb, M. A., Cheeseman, J. R., Scalmani, G., Barone, V., Petersson, G. A., Nakatsuji, H., Li, X., Caricato, M., Marenich, A. V., Bloino, J., Janesko, B. G., Gomperts, R., Mennucci, B., Hratchian, H. P., Ortiz, J. V., Izmaylov, A. F., Sonnenberg, J. L., Williams-Young, D., Ding, F., Lipparini, F., Egidi, F., Goings, J., Peng, B., Petrone, A., Henderson, T., Ranasinghe, D., Zakrzewski, V. G., Gao, J., Rega, N., Zheng, G., Liang, W., Hada, M., Ehara, M., Toyota, K., Fukuda, R., Hasegawa, J., Ishida, M., Nakajima, T., Honda, Y., Kitao, O., Nakai, H., Vreven, T., Throssell, K., Montgomery, J. J. A., Peralta, J. E., Ogliaro, F., Bearpark, M. J., Heyd, J. J., Brothers, E. N., Kudin, K. N., Staroverov, V. N., Keith, T. A., Kobayashi, R., Normand, J., Raghavachari, K., Rendell, A. P., Burant, J. C., Iyengar, S. S., Tomasi, J., Cossi, M., Millam, J. M., Klene, M., Adamo, C., Cammi, R., Ochterski, J. W., Martin, R. L., Morokuma, K., Farkas, O., Foresman, J. B., Fox, D. J.: Gaussian 16, Revision A.03, Gaussian, Inc., Wallingford, (2016)
39. Zhao, Y., Truhlar, D.G.: Design of density functionals that are broadly accurate for thermochemistry, thermochemical kinetics, and nonbonded interactions. J. Phys. Chem. A. **109**, 5656–5667 (2005)
40. Goerigk, L., Hansen, A., Bauer, C., Ehrlich, S., Najibi, A., Grimme, S.: A look at the density functional theory zoo with the advanced GMTKN55 database for general main group thermochemistry, kinetics and noncovalent interactions. Phys. Chem. Chem. Phys. **19**, 32184–32215 (2017)
41. Garrett, B.C., Truhlar, D.G.: Generalized transition state theory. Classical mechanical theory and applications to collinear reactions of hydrogen molecules. J. Phys. Chem. **83**, 1052–1079 (1979)
42. Miyoshi, A.: GPOP software, rev. 2013.07.15m7, Available at http://akrmys.com/gpop/. Accessed 12 Feb 2018
43. Zubarev, R.A.: Reactions of polypeptide ions with electrons in the gas phase. Mass Spectrom. Rev. **22**, 57–77 (2003)
44. Kohtani, M., Jarrold, M.F., Wee, S., O'Hair, R.A.: Metal ion interactions with polyalanine peptide. J. Phys. Chem. B. **108**, 6093–6097 (2004)
45. Moon, J.H., Yoon, S., Bae, Y.J., Kim, M.S.: Formation of gas-phase peptide ions and their dissociation in MALDI: insights from kinetic and ion yield studies. Mass Spectrom. Rev. **34**, 94–115 (2015)
46. Diedrich, J.K., Julian, R.R.: Site-specific radical directed dissociation of peptides at phosphorylated residues. J. Am. Chem. Soc. **130**, 12212–12213 (2008)
47. Sun, Q., Nelson, H., Ly, T., Stoltx, B.M., Julian, R.R.: Side chain chemistry mediates backbone fragmentation in hydrogen deficient peptide radicals. J. Proteome Res. **8**, 958–966 (2009)